Dyes and Pigments 157 (2018) 328–333

Contents lists available at ScienceDirect

Dyes and Pigments

journal homepage: www.elsevier.com/locate/dyepig

A mitochondria-targeting fluorescent Fe^{3+} probe and its application in labile Fe^{3+} monitoring via imaging and flow cytometry

Chengcheng Zhu[a], Mengjia Wang[a], Lin Qiu[a,b,**], Shuangying Hao[c], Kuanyu Li[c,***], Zijian Guo[a], Weijiang He[a,*]

[a] State Key Laboratory of Coordination Chemistry, School of Chemistry and Chemical Engineering, Nanjing University, Nanjing 210023, China
[b] School of Pharmaceutical Engineering and Life Science, Changzhou University, Changzhou 213164, China
[c] Jiangsu Key Laboratory of Molecular Medicine, Medical School of Nanjing University, Nanjing 210093, China

A B S T R A C T

The biogenesis of heme and iron-sulfur cluster in mitochondria is closely associated with the intracellular iron homeostasis. In this study, a mitochondria-targeting probe with the reversible turn-on fluorescent response to Fe^{3+} was developed for mitochondrial labile Fe^{3+} monitoring by modifying spirolactam rhodamine with a chelator. With this probe, the mitochondrial labile Fe^{3+} fluctuation in adherent cells upon ferric citrate incubation was visualzied via confocal imaging, and the flow cytometric assay for mitochondrial Fe^{3+} in suspension cells, which is difficult to be monitored via confocal imaging, was also developed. Moreover, the labile Fe^{3+} drop in mitochondria of K562 cells undergoing the DMSO-stimulated erythroid differentiation was observed for the first time.

1. Introduction

Iron plays essential roles in biological processes of eukaryotic cells such as oxygen transport [1], electron transfer [2], and enzymatic catalysis [3]. Most of these functions were associated with mitochondria, which are proposed as iron reservoir and metabolism site in cells. The biogenesis of heme and iron-sulfur clusters are the most important iron-related events in mitochondria [4], and the Fe-S clusters are essentially involved in Iron Regulatory Protein 1 (IRP1) which regulates the intracellular iron homeostasis. In addition, the dysregulation of mitochondrial iron has been reported to induce ROS generation and mitochondrial membrane lipid peroxidation, which results in diseases such as Parkinson's disease, Alzheimer's disease, and Friedreich's ataxia [5]. The newly discovered type of cell death, ferroptosis, shows also the increased mitochondrial membrane as one of its characteristics [6]. How to understand the physiological processes of iron homeostasis to sustain mitochondrial functions demands reliable technique to sense mitochondria iron perturbation. Since the isotope labelling and X-ray related analysis are difficult to offer in situ iron information in live cells [7], fluorescence imaging, which is able to offer in situ spatial-temporal information of chemical species in live systems, has been proposed for labile (or chelatable) Fe^{3+} monitoring in cells to evaluate the intracellular iron homeostasis [4,8,9], although most iron exists in bound state. However, the fluorescence sensing of Fe^{3+} is still challenging owning to the paramagnetic nature of Fe^{3+} quenching fluorescence critically. In fact, the fluorescent probe for mitochondrial labile Fe^{3+} is rare [10], and the ROS probe dihydrorhodamine 123 has been adopted for indirect sensing of mitochondrial labile iron fluctuation in the study of Friedreich's ataxia, since Fe^{3+} induces ROS generation in cells [11].

In this study, a new rhodamine-based fluorescent probe for Fe^{3+}, **Mito-RhFe** (Scheme 1), was developed for mitochondrial labile Fe^{3+} sensing in living cells. In this probe, spirolactam rhodamine was adopted as fluorescence signaling group due to its turn-on response triggered by target-induced ring opening process [12]. Moreover, the delocalized positive charge of rhodamine is expected to favor the mitochondrion targeting ability [13]. N^2-hydroxyethyldiethylenetriamine (HEDTA) was incorporated as a chelator due to its fine Fe^{3+} affinity [14]. This new probe shows not only the Fe^{3+}-specific turn-on fluorescent response but also the distinct mitochondrion target ability in live cells. The mitochondrial labile Fe^{3+} imaging in adherent cells and flow cytometric assay for labile Fe^{3+} in mitochondria of suspension cells were realized with this probe.

* Corresponding author. State Key Laboratory of Coordination Chemistry, School of Chemistry and Chemical Engineering, Nanjing University, Nanjing 210023, China.
** Corresponding author. School of Pharmaceutical Engineering and Life Science, Changzhou University, Changzhou 213164, China.
*** Corresponding author. Jiangsu Key Laboratory of Molecular Medicine, Medical School of Nanjing University, Nanjing 210093, China.
E-mail addresses: linqiu@cczu.edu.cn (L. Qiu), likuanyu@nju.edu.cn (K. Li), heweij69@nju.edu.cn (W. He).

https://doi.org/10.1016/j.dyepig.2018.05.008
Received 10 February 2018; Received in revised form 5 May 2018; Accepted 5 May 2018
Available online 07 May 2018
0143-7208/ © 2018 Elsevier Ltd. All rights reserved.

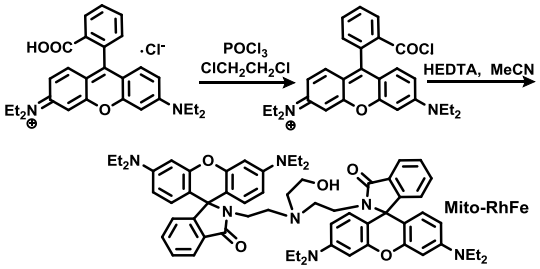

Scheme 1. Synthesis of probe **Mito-RhFe**. Reagents and conditions: (i) $POCl_3$, 1, 2-dichloroethane, reflux, 4 h (ii) HEDTA, acetonitrile, RT, overnight.

2. Experimental

2.1. Materials, general methods and instrumentations

Solvents and reagents were commercial available and used without further purification. All solvents for spectroscopic study were of spectrum grade. Water for spectroscopic determination is the deionized water from MilliQ system (> 18 MΩ). All fluorescence spectra were recorded using Horiba Scientific Fluoromax-4 fluorescence spectrophotometer, while the UV/Vis absorption spectra were recorded on a LAMBDA-35 spectrophotometer. All NMR spectra were recorded with Bruker DRX-500 or Bruker DRX-300. All the pH values were record using a pH meter Sartorius PB-10 meter. High resolution mass spectrometric data were determined using an Agilent 6540 Q-TOF HPLC-MS spectrometer. All the antibodies for western-blotting such as rabbit anti-MFRN1 (Abcam), rabbit anti-MFRN2 (Abcam), rabbit anti-globin (Abcam), mouse anti-GAPDH (proteintech) were commercial available. HPLC analysis of **Mito-RhFe** (10 μM) in Tris-HCl buffer was carried out with SHIMADZU LC-20AT using a AcclaimTM 120C18 column (5 μm, 120 Å, 4.6*250 mm). The column temperature was at 30°C, the UV detection wavelength was 550 nm, and the mobile phase was the mixed solvent of CH_3OH and H_2O (9:1, v/v).

2.2. Synthesis ***Mito-RhFe*** (Scheme 1)

2.2.1. Synthesis of rhodamine B chloride

Rhodamine B (1.0 g, 2.3 mmol) was dissolved in 1,2-dichloroethane (12 mL) and $POCl_3$ (0.6 mL) was added dropwise in 5 min. Then the mixture was refluxed with stirring for 4 h. After being cooled to room temperature, the mixture was evaporated in vacuo to remove solvent, and the resulted residual can be utilized as the raw material for **Mito-RhFe** preparation directly.

2.2.2. Synthesis of 1-bis(1-aminoethyl)amino ethanol (HEDTA)

Diethylenetriamine (150 g, 1454 mmol) and concentrated sulfuric acid (93 mL) were mixed in water followed by adding ethylene oxide (30 g, 681.0 mmol) slowly in 1 h. Then the mixture was stirred at room temperature overnight. The mixture was poured into 400 g NaOH solution (50%), and the precipitate was filtered off. The filtrate was extracted with isopropyl alcohol, and the combined extracts were combined and evaporated in vacuo. The residue was distilled in vacuo and the fraction collected at 148°C/11 mmHg is the final product. Yield, 13%. ^{1}H NMR (400 MHz, $CDCl_3$, δ, ppm): 3.35 (t, J = 4.0 Hz, 2H), 2.52 (t, J = 6.0 Hz, 4H), 2.37 (t, J = 4.0 Hz, 2H), 2.33 (t, J = 6.0 Hz, 4H), 1.99 (br, 4H).

2.2.3. Synthesis of ***Mito-RhFe***

Rhodamine B chloride (1.07 g, 2.3 mmol) was dissolved in acetonitrile, and **HEDTA** (5 mL in 20 mL acetonitrile) was added dropwise into the solution in 1 h at 0 °C. The resulted mixture was stirred at room temperature overnight. Then the solvent was removed in vacuo. Washing the residue with water (20 mL × 4), and the solid was purified by chromatographic column (CH_2Cl_2:CH_3OH = 20:1, v/v), and the product **Mito-RhFe** was obtained as orange solid. Yield, 20%. ^{1}H NMR (500 MHz, $CDCl_3$, δ, ppm): 7.87 (m, Ar-H, 2H), 7.43 (m, Ar-H, 4H), 7.08 (m, Ar-H, 2H), 6.38 (m, Ar-H, 8H), 6.28 (m, Ar-H, 4H), 3.34 (q, J = 7.08 Hz, 16H), 3.11 (t, J = 4.56 Hz, 2H), 3.04 (t, J = 7.12 Hz, 4H), 2.19 (m, 6H), 1.17 (t, J = 7.00 Hz, 24H). ^{13}C NMR (126 MHz, $CDCl_3$, δ, ppm): 167.56, 153.45, 153.24, 148.8, 132.06, 131.73, 128.88, 127.90, 123.74, 122.64, 108.20, 105.82, 97.88, 64.95, 58.81, 55.44, 51.77, 44.34, 38.16, 12.61. HR-MS (positive mode, m/z): Calcd. 996.5751, found 996.5749 for $[M+H]^+$.

2.3. Colocalization of Mito-RhFe with MitoTracker Deep Red 633 in MCF-7 cells and HeLa cells

MCF-7 and HeLa cells were cultured respectively in DMEM supplemented with 10% FBS (fetal calf bovine serum) in an atmosphere of 5% CO_2 and 95% air at 37°C. The cells were stained with **Mito-RhFe** (10 μM, 0.5 h) in PBS (1 ×) at ambient temperature. The staining medium was prepared by adding the stock solution of **Mito-RhFe** in DMSO into PBS buffer to the desired concentration (10 μM) and the maximum DMSO content in the final solution was lower than 0.2%. After the first imaging, the cells were stained further with MitoTracker Deep Red 633 (1 μM, 5 min) at ambient temperature for the second imaging. All the imaging was carried out with dual channel model (**Mito-RhFe** channel: bandpass 570–620 nm, λ_{ex} = 543 nm; MitoTracker channel: bandpass 665–730 nm, λ_{ex} = 633 nm). The imaging was realized with a confocal laser scanning fluorescence microscope (Zeiss LSM710).

2.4. Confocal fluorescence imaging for intracellular labile Fe^{3+} in living cells

HeLa cells were cultured in DMEM supplemented with 10% FBS (fetal calf bovine serum) in an atmosphere of 5% CO_2 and 95% air at 37 °C. The cells were stained with **Mito-RhFe** (10 μM, 30 min at ambient temperature). After imaging, the cells were incubated further with ferric citrate (20 μM) in PBS for 0.5 h. After the second imaging, the cells were further incubated with TPEN (50 μM) in PBS for 0.5 h at room temperature for imaging. The imaging was carried out using a confocal fluorescence microscope (Zeiss LSM710) with a bandpass of 570–620 nm upon excitation at 543 nm.

2.5. Flow cytometric assay for exogenous labile Fe^{3+} in MEL cells

MEL cells were seeded in 60 mm dishes with the number of 5×10^5 and cultured with DMEM supplemented with 10% FBS (fetal bovine serum) in an atmosphere of 5% CO_2 and 95% air at 37 °C for 24 h. Then different concentration of ferric citrate (0, 10, 20, 40, and 50 μM) was added respectively into the medium to culture the cells for 6 h. After that, the cells were collected and rinsed with PBS for 3 times. Then the cells were stained with **Mito-RhFe** (10 μM, 0.5 h) in PBS cooled by ice. After removing the staining medium, the cells were rinsed by PBS for 3 times and resuspended in PBS for flow cytometric assay with a flow cytometer (BD LSR Fortessa™) using PE channel.

2.6. Flow cytometric assay for endogenous labile Fe^{3+} in stimulated K562 cells

The cells were seeded in 35 mm dishes with a density of 1×10^4 per dish and cultured for 4 days in RPMI 1640 medium (Hyclone, USA) containing 2% DMSO (Sigma, v/v), 10% fetal bovine serum (FBS), 100 U/ml penicillin and 100 μg/mL streptomycin at 37 °C in incubator containing a humid atmosphere of 5% CO_2 and 95% air. The medium was replaced every two days, and 50 μM ferric citrate was added to the medium on second day after each replacement. Then the cells were treated respectively for Western blot analysis and flow cytometric

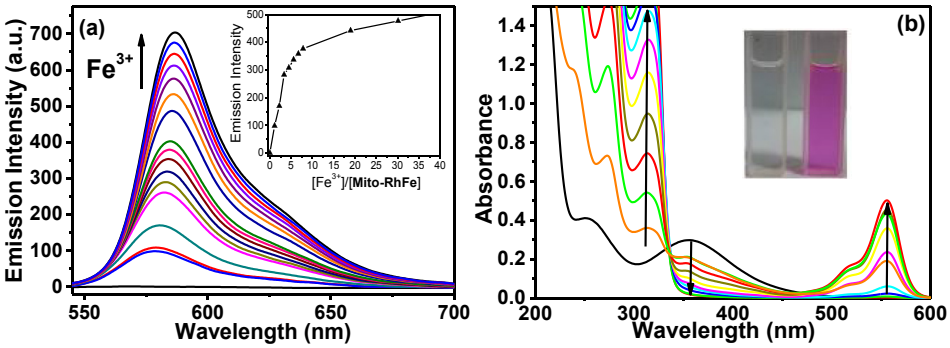

Fig. 1. Emission (a, λ_{ex} = 540 nm) and absorption (b) spectra of **Mito-RhFe** (10 μM) in Tris-HCl buffer (20 mM, pH 7.20, 50% methanol, v/v) upon titration with Fe^{3+} (0–20 equiv). Inset in (a): Titration profile according to the emission at 580 nm. Inset in (b): photograph of **Mito-RhFe** solution before (left) and after (right) Fe^{3+} addition.

assay. For Western blot analysis, the cells were suspended in RIPA lysis buffer to quantify the target protein expression use 12% SDS-PAGE gels. The antibodies were used following the user guide. The flow cytometric assay was carried out in the procedure described in 2.5. The control without 2% DMSO was also carried out for comparison.

3. Results and discussion

3.1. Fluorescent response of probe *Mito-RhFe* to Fe^{3+} in solution

The solution of compound **Mito-RhFe** (10 μM) in Tris-HCl buffer (20 mM, pH 7.2, 50% methanol, v/v) displays almost no fluorescence but the typical absorption bands at 205, 250 and 355 nm of spirlolactam form for rhodamine. The rhodamine emission band centered at 578 nm appears and increases with a ~8 nm bathochromic shift upon Fe^{3+} titration and excitation at 540 nm (Fig. 1a). The fluorescence enhancement factor, $(F\text{-}F_0)/F_0$, attains to ~90-fold upon titration with 20 equiv of Fe^{3+}. In UV-vis Fe^{3+} titration of this probe, the absorption spectra show the distinct drop of its absorption band at 355 nm, and the increase of new bands centered respectively at 273 and 314 nm. Moreover, an absorption band at 555 nm appears distinctly with a shoulder at 517 nm (Fig. 1b). This band is the characterized absorption of rhodamine in ring open form. In the meantime, the color of **Mito-RhFe** solution changes from colorless to magenta (Fig. 1b inset). All these phenomena are consistent with the expected conversion of **Mito-RhFe** from spirolactam to ring opening form.

The fluorescent response of **Mito-RhFe** (10 μM) to metal cations of interest has been investigated via determining the emission spectra of **Mito-RhFe** (Fig. 2a). The spectra indicate that most of the tested metal cations such as Fe^{2+}, Hg^{2+}, Cd^{2+}, Zn^{2+}, Pb^{2+}, Co^{2+}, Ag^{+}, Cu^{2+}, Mn^{2+}, Ni^{2+} (20 equiv) and K^{+}, Mg^{2+},Ca^{2+} and Na^{+} (100 equiv) do not induce the fluorescence of **Mito-RhFe**, yet Fe^{3+}, Cr^{3+} and Al^{3+} (20 equiv) increase the probe fluorescence with the enhancement factors of 90-, 6-, and 14-fold, respectively. With the scarcity of Cr^{3+} and Al^{3+} in living systems, the emission enhancement induced by Cr^{3+} and Al^{3+} does not affect the Fe^{3+} sensing behavior of **Mito-RhFe** in cells. Moreover, the presence of most tested metal cation does not interfere with the turn-on response of **Mito-RhFe** to Fe^{3+}, except for Cd^{2+}, Zn^{2+}, and Ni^{2+} reducing the Fe^{3+}-induced emission enhancement factors respectively to ~58-, 50-, and 40-fold. In addition, the Fe^{3+}-induced emission enhancement of **Mito-RhFe** can be reduced distinctly by adding TPEN (*N,N,N′,N′-tetrakis*(2-pyridylmethyl)-ethylenediamine, 20 equiv), a cell membrane permeable transition metal chelator (Fig. 2b). The second Fe^{3+} addition to probe solution shows again the enhanced emission similar to that upon first addition. Therefore, the Fe^{3+} sensing behavior of probe **Mito-RhFe** is reversible in general. This reversible response has also been confirmed by HPLC analysis. It was found that **Mito-RhFe** showed only one signal of retention time 6.88 min for the spirolactam form (100% area), and Fe^{3+} addition led to the second signal of retention time 5.44 min besides the signal of the spirolactam form. Considering the turn-on response in UV-vis and emission spectra induced by Fe^{3+}, this new signal could be assigned to the ring open form of **Mito-RhFe** bound with Fe^{3+}. The subsequent treatment with TPEN to remove Fe^{3+} made almost all the new signal transit to the former signal for spirolactam form, demonstrating the recovery of spirolactam from the ring open form (Fig. S5). The fluorescence detection limit of this probe is determined as 1.07×10^{-7} M (Fig. S6) via titration experiment. In addition, the turn-on response of this probe can be fulfilled with Fe^{3+} in ~200 s (Fig. S7). In the pH range from 6.0 to 12.3, this probe shows almost no fluorescence (Fig. S8), and the distinct fluorescence enhancement of **Mito-RhFe** only can be observed when medium pH is lower than pH 5.0. This implies that the ring opening process of this spirolactam probe occurs only at pH < 5.0. The pH-independent stability of this spirolactam probe in pH 6.0–12.3 suggests **Mito-RhFe** is suitable for Fe^{3+} sensing in mitochondria, which possesses a slightly basic microenvironment of pH of ~8.0, providing the colocalization experiment disclosing the mitochondrion-preferring distribution of **Mito-RhFe** (*vide infra*).

3.2. Fluorescence imaging of mitochondrial labile Fe^{3+} in live cells via *Mito-RhFe* staining

Fluorescence imaging of **Mito-RhFe** has been investigated in live cells such as MCF-7 and HeLa cells with a confocal laser scanning

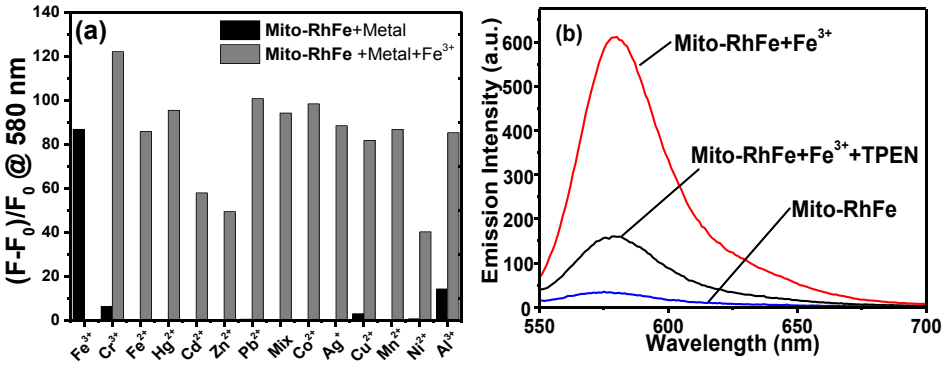

Fig. 2. (a) Fluorescent response of **Mito-RhFe** (10 μM) to Fe^{2+}, Hg^{2+}, Cd^{2+}, Zn^{2+}, Pb^{2+}, Co^{2+}, Ag^{+}, Cu^{2+}, Mn^{2+}, Ni^{2+} (200 μM), and K^{+}, Mg^{2+},Ca^{2+}, and Na^{+} (1000 μM) in Tris-HCl buffer (20 mM, pH 7.20, 50% methanol, v/v) with (grey) or without (black) the presence of Fe^{3+} (200 μM). $(F\text{-}F_0)/F_0$ was calculated based on the emission at 580 nm. (b) Fluorescence spectra of **Mito-RhFe** (10 μM) obtained as free probe, in the presence of 20 equiv Fe^{3+}, and after the subsequent TPEN (200 μM) addition. λ_{ex} = 540 nm.

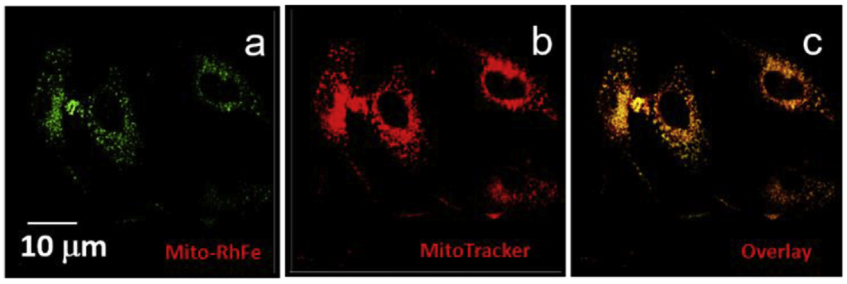

Fig. 3. Colocalization of **Mito-RhFe** with MitoTracker Deep red 633 in MCF-7 cells. The cells were stained firstly by 10 μM probe in PBS for 30 min at 37 °C. After the first imaging, the cells were incubated further with 1 μM MitoTracker Deep Red 633 (5 min) in PBS at 37 °C for the second imaging. (a) fluorescence image of cells recorded in first imaging with a bandpass of 570–620 nm upon excitation at 543 nm; (b) fluorescence image of cells in (a) recorded in second imaging with a bandpass of 665–730 nm upon excitation at 633 nm (c) Overlay of (a) and (b). (For interpretation of the references to color in this figure legend, the reader is referred to the Web version of this article.)

microscope (Zeiss LSM710). The imaging shows the weak fluorescence in cytosol after 30 min of incubation with **Mito-RhFe**, while cells without probe incubation show no fluorescence in the same condition. This indicates the fine cell membrane permeability of this probe. Colocalization with MitoTracker Deep Red 633 in MCF-7 cells discloses that the intracellular fluorescence of **Mito-RhFe** recorded in probe channel is localized on mitochondria visualized by MitoTracker fluorescence recorded in MitoTracker channel (Fig. 3). The Pearson's colocalization coefficient of **Mito-RhFe** with MitoTracker was 0.96. Colocalization in HeLa cells discloses also the mitochondria-targeting ability with a coefficient of ~0.90.

With the mitochondrion targeting ability, **Mito-RhFe** was utilized to visualize mitochondrial labile Fe^{3+} fluctuation in HeLa cells upon Fe^{3+} incubation by imaging (Fig. 4). The confocal imaging displays the weak fluorescent dots (Fig. 4b), indicating the low mitochondrial labile Fe^{3+} level. After being incubated with ferric citrate (20 μM) for 30 min, the cells show the distinctly enhanced fluorescence (Fig. 4c), suggesting the labile Fe^{3+} level in mitochondria can be effectively enhanced by exogenous Fe^{3+} incubation. The subsequent incubation with TPEN makes the fluorescence in mitochondria even lower than that shown in Fig. 4b. This demonstrates the labile Fe^{3+} in mitochondria can be effectively removed by TPEN scavenging (Fig. 4d). All these indicate that the labile Fe^{3+} fluctuation in mitochondria can be effectively monitored in a reversible manner by **Mito-RhFe**.

3.3. *Flow cytometric assay for mitochondrial labile Fe^{3+} in suspension cells via **Mito-RhFe** staining*

With the successful imaging for labile Fe^{3+} in adherent cells, **Mito-RhFe** was further investigated for its flow cytometric application in sensing mitochondrial labile Fe^{3+} in suspension cells. Since the suspension cells, such as the blood cells, can't be monitored by confocal fluorescence imaging, the flow cytometric assay for labile Fe^{3+} instead of confocal imaging becomes the promising alternative for fluorescence sensing of labile Fe^{3+} in suspension cells, especially the mitochondrial iron metabolism is of great significance for blood cells. Therefore mouse erythroleukaemia (MEL) cells were incubated respectively with ferric citrate solutions of different concentration (0–50 μM, 6 h at 37 °C) followed by staining with probe solution (10 μM, 30 min at 0 °C). The stained cells were determined by a flow cytometer using a PE channel. The determined cell population distribution discloses the fluorescence for population maximum increases distinctly with the ferric citrate concentration if the ferric citrate concentration attains to 20 μM (Fig. 5a), although 10 μM ferric citrate incubation induces no difference from the control without Fe^{3+} incubation. The median fluorescence determined at different ferric citrate concentration shows also that ferric citrate incubation will increase the labile Fe^{3+} level in mitochondria of MEL cells (Fig. 5b). All the results imply **Mito-RhFe** can be practically applied in sensing mitochondrial labile Fe^{3+} in suspension cells via flow cytometry.

Erythroid differentiation is essential for erythropoiesis from hematopoietic stem cell [15], and artificial stimulated erythroid differentiation is normally adopted in lab to explore the complicated physiological network involved erythropoiesis. The differentiation is usually accompanied by distinct hemoglobin synthesis and upregulation of the mitochondrial iron importing protein Mitoferrin-1 (MFRN1) containing Fe-S cluster [4,16], and maturation is normally confirmed by benzidine staining to show the distinctly upregulated level of hemoglobin [7a,17]. Since hemoglobin and Fe-S cluster biogenesis in erythropoiesis is closely associated with mitochondrial iron accumulation and incorporation [4a,18], the labile Fe^{3+} perturbation in mitochondria can be expected. The success of flow cytometric assay of mitochondrial labile Fe^{3+} via **Mito-RhFe** staining inspires us to explore the possibility to monitor erythroid differentiation process via sensing mitochondria labile Fe^{3+} levels in the stimulated leukemic cells. The human K562 erythroleukemia cells, the common model for erythroid progenitors upon stimulation with many stimulatory factors such as DMSO [19,20], were cultured in medium with 2% DMSO for 4 days for labile Fe^{3+} flow cytometric assay. The results disclose that the median fluorescence of the DMSO-stimulated cells is distinctly decreased when compared with that of the control without DMSO stimulation (Fig. 6a). On the other hand, the western blot results show that DMSO stimulation leads to the distinct hemoglobin expression in the cells, while the control without DMSO induction shows almost no this protein (Fig. 6b). In addition, the obviously enhanced MFRN1 was also observed upon DMSO stimulation. All the western blot results confirm the erythrocyte maturation stimulated by culturing K562 cells for 4 days in DMSO-containing RPMI-1640 medium. The accompanied median fluorescence decrease in flow cytometric assay suggests the stimulated synthesis of heme and Fe-S cluster in mitochondria may consume too much iron in mitochondria which decreases the labile Fe^{3+} level in mitochondria, and the mitochondrial labile Fe^{3+} monitoring via flow cytometry might be an effective tool for the assessment of erythroid differentiation.

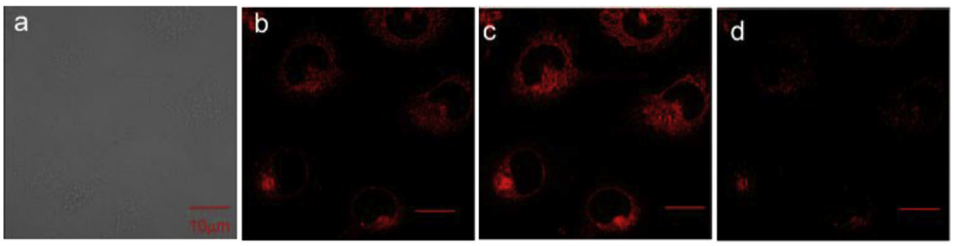

Fig. 4. Confocal fluorescence imaging of HeLa cells stained by **Mito-RhFe** (10 μM in PBS, 30 min at 37 °C). (a) Bright field cell image; (b) fluorescence image of the stained cells; (c) fluorescence image of the cells in (b) incubated further with ferric citrate (20 μM, 30 min at 37 °C); (d) fluorescence image of cells in (c) treated further with TPEN (50 μM, 30 min at 37 °C) incubation. λ_{ex} = 543 nm, bandpass: 560–620 nm. Scale bar, 10 μm.

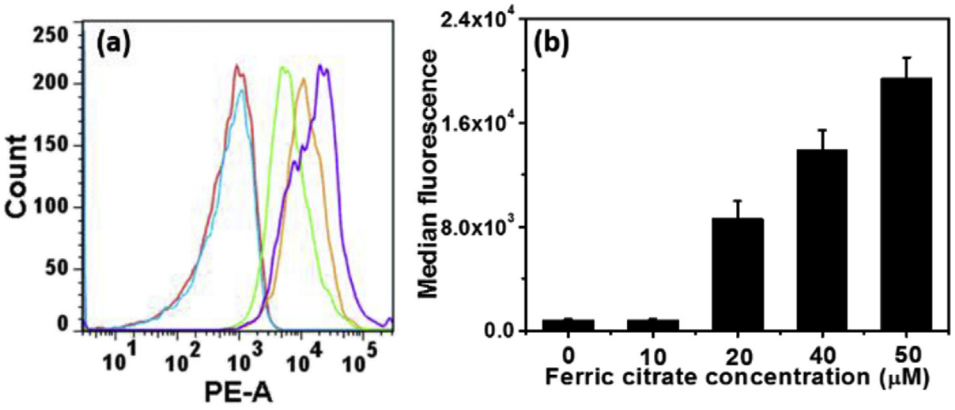

Fig. 5. Flow cytometric assay of MEL cells incubated with ferric citrate solutions of different concentration for 6 h (37 °C), followed by incubation with **Mito-RhFe** (10 μM, 30 min, 0 °C). Test was realized with a PE channel. (a) Histogram of MEL cells incubated with Fe^{3+} of 0 (red), 10 (blue), 20 (green), 40 (yellow), and 50 (purple) μM. (b) Median fluorescence of the stained MEL cells induced by Fe^{3+} incubation shown in (a). (For interpretation of the references to color in this figure legend, the reader is referred to the Web version of this article.)

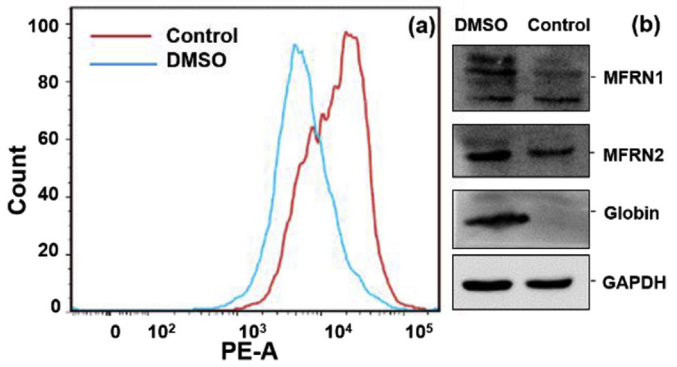

Fig. 6. (a) Labile Fe^{3+} flow cytometric assay of K562 cells incubated in RPMI-1640 medium containing 2% DMSO. (b) Western blot analysis of the cells in (a). The cells were cultured at 37 °C for 4 days, and stained with **Mito-RhFe** at 0 °C for 30 min before assay. Cells cultured without DMSO were adopted as the control.

4. Conclusion

In summary, the newly prepared **Mito-RhFe** shows the specific turn-on response to Fe^{3+}. Its reversible response makes this probe more effective than normal chemodosimeters with turn-on response to Fe^{3+}. Confocal imaging via **Mito-RhFe** staining confirms the probe's mitochondria-targeting ability and capability to visualize reversibly the mitochondrial labile Fe^{3+} fluctuation in adherent cells such as HeLa cells triggered by ferric citrate incubation. Besides the ability to sense the exogenous mitochondrial labile Fe^{3+} oscillation in suspension cells, the Fe^{3+} flow cytometry based on **Mito-RhFe** has disclosed the decreased endogenous labile Fe^{3+} level in mitochondria of the erythroid differentiated K562 cells stimulated by DMSO. This infers the flow cytometry assay based on **Mito-RhFe** may be an effective supplementary method to evaluate the erythroid differentiation of leukemic cells. To improve the probe selectivity and sensitivity for mitochondrial labile Fe^{3+} sensing, screening more specific Fe^{3+} chelators to construct probes in the strategy based on spirolactam rhodamine is still undergoing.

Acknowledgements

We thank the financial supports from the National Basic Research Program of China (No. 2015CB856300), National Natural Science Foundation of China (Nos: 21571099 and 21731004) and Natural Science Foundation of Jiangsu (No: BK20150054) for financial support.

Appendix A. Supplementary data

Supplementary data related to this article can be found at http://dx.doi.org/10.1016/j.dyepig.2018.05.008.

References

[1] (a) Aisen P, Wessling-Resnick M, Leibold EA. Iron metabolism. Curr Opin Chem Biol 1999;3:200;
(b) Connie MD, Hsia CW. Respiratory function of hemoglobin. N Engl J Med 1998;338:239.

[2] (a) Netz DJA, Stümpfig M, Doré C, Mühlenhoff U. Tah18 transfers electrons to Dre2 in cytosolic iron-sulfur protein biogenesis. Nat Chem Biol 2010;6:758;
(b) Murataliev MB, Feyereisen R, Walker FA. Electron transfer by diflavin reductases. Biochim Biophys Acta 2004;1698:1;
(c) Lucas MF, Rousseau DL, Guallar V. Electron transfer pathways in cytochrome c oxidase. Biochim Biophys Acta 2011;1807:1305.

[3] (a) Eisenstein RS. Iron regulatory proteins and the molecular control of mammalian iron metabolism. Annu Rev Nutr 2000;20:627;
(b) Rouault TA. The role of iron regulatory proteins in mammalian iron homeostasis and disease. Nat Chem Biol 2006;2:406.

[4] (a) Kafina MD, Paw BH. Intracellular iron and heme trafficking and metabolism in developing erythroblasts. Metall 2017;9:1193;
(b) Braymer JJ, Lill R. Iron–sulfur cluster biogenesis and trafficking in mitochondria. J Biol Chem 2017;292:12754;
(c) Lill R. Function and biogenesis of iron–sulphur proteins. Nature 2009;460:831.

[5] (a) Huang ML-H, Becker EM, Whitnall M. Elucidation of the mechanism of mitochondrial iron loading in Friedreich's ataxia by analysis of a mouse mutant. Proc Natl Acad Sci USA 2009;106:16381;
(b) Whitnall M, Rahmanto YS, Sutak R. The MCK mouse heart model of Friedreich's ataxia: alterations in iron-regulated proteins and cardiac hypertrophy are limited by iron chelation. Proc Natl Acad Sci USA 2008;105:9757;
(c) Huang ML-H, Lane DJR, Richardson DR. Mitochondrial mayhem: the mitochondrion as a modulator of iron metabolism and its role in disease. Antioxidants Redox Signal 2011;15:3003.

[6] (a) Yu H, Guo P, Xie X. Ferroptosis, a new form of cell death, and its relationships with tumourous diseases. J Cell Mol Med 2017;21:648;
(b) Dixon SJ, Lemberg KM, Lamprecht MR. Ferroptosis: an iron-dependent form of nonapoptotic cell death. Cell 2012;149:1060.

[7] (a) Friend C, Scher W, Holland JG. Hemoglobin synthesis in murine virus-induced leukemic cells in vitro: stimulation of erythroid differentiation by dimethyl sulfoxide. Proc Natl Acad Sci USA 1971;68:378;
(b) Fahrni CJ. Biological applications of X-ray fluorescence microscopy: exploring the subcellular topography and speciation of transition metals. Curr Opin Chem Biol 2007;11:121.

[8] (a) Que EL, Domaille DW, Chang CJ. Metals in neurobiology: probing their chemistry and biology with molecular imaging. Chem Rev 2008;108:1517;
(b) Liu Z, He W, Guo Z. Metal coordination in photoluminescent sensing. Chem Soc Rev 2013;42:1568.

[9] (a) Zhu H, Fan J, Wang B. Fluorescent, MRI, and colorimetric chemical sensors for the first-row d-block metal ions. Chem Soc Rev 2015;44:4337;
(b) Sahoo SK, Sharma D, Bera RK. Iron(III) selective molecular and supramolecular fluorescent probes. Chem Soc Rev 2012;41:7195.

[10] Chen W, Gong W, Ye Z. FRET-based ratiometric fluorescent probes for selective Fe^{3+} sensing and their applications in mitochondria. Dalton Trans 2013;42:10093.

[11] Kakhlon O, Manning H, Breuer W. Cell functions impaired by frataxin deficiency are restored by drug-mediated iron relocation. Blood 2008;112:5219.

[12] (a) Kim HN, Lee MH, Kim HJ, Yoon J. A new trend in rhodamine-based chemosensors: application of spirolactam ring-opening to sensing ions. Chem Rev Soc 2008;37:1465;
(b) Lee HY, Swamy KMK, Jung JY, Kim G, Jung JY. Rhodamine hydrazone derivatives based selective fluorescent and colorimetric chemodosimeters for Hg^{2+} and selective colorimetric chemosensor for Cu^{2+}. Sensor Actuator B Chem 2013;182:530;
(c) Beija M, Afonso CAM, Martinho JMG. Synthesis and applications of Rhodamine derivatives as fluorescent probes. Chem Soc Rev 2009;38:2410,;
(d) Yang Y-K, Yook K-J, Tae J. A rhodamine-based fluorescent and colorimetric chemodosimeter for the rapid detection of Hg^{2+} ions in aqueous media. J Am Chem Soc 2005;127:16760.

[13] (a) Johnson LV, Walsh ML, Chen LB. Localization of mitochondria in living cells with rhodamine 123. Proc Natl Acad Sci USA 1980;77:990;
(b) Johnson LV, Walsh ML, Bockus BJ. Monitoring of relative mitochondrial membrane potential in living cells by fluorescence microscopy. J Cell Biol 1981;88:526;
(c) Kim YK, Ha H, Lee J. Control of muscle differentiation by a mitochondria-targeted fluorophore. J Am Chem Soc 2010;132:576.
[14] Qiu L, Zhu C, Chen H. A turn-on fluorescent Fe^{3+} sensor derived from an anthracene-bearing bisdiene macrocycle and its intracellular imaging application. Chem Commun 2014;50:4631.
[15] Dzierzak E, Philipsen S. Erythropoiesis: development and differentiation. Cold Spring Harbor. Perspect. Med 2013;3:a011601.
[16] Shaw GC, Cope JJ, Li L. Mitoferrin is essential for erythroid iron assimilation. Nature 2006;440:96.
[17] Deezagi M. Abeditashi, Studying the enucleation process, DNA breakdown and telomerase activity of the K562 cell lines during erythroid differentiation in vitro. In Vitro Cell Dev Biol Anim 2013;49:122.
[18] Fontenay M, Cathelin S, Amiot M. Mitochondria in hematopoiesis and hematological diseases. Oncogene 2006;25:4757.
[19] Toobiak Shlomi, Shaklai Mati, Shaklai Nurith. Carbon monoxide induced erythroid differentiation of K562 cells mimics the central macrophage milieu in erythroblastic islands. PLoS One 2012;7:e33940.
[20] (a) Andersson LC, Jokinen M, Gahmberg CG. Induction of erythroid differentiation in the human leukaemia cell line K562. Nature 1979;278:364;
(b) Rutherford TR, Clegg JB, Weatherall DJ. K562 human leukaemic cells synthesise embryonic haemoglobin in response to haemin. Nature 1979;280:164.

Chengcheng Zhu is a PhD candidate of Nanjing University. His research focuses on the fluorescent sensing and imaging for transition metal cations in live cells and animal models.

Mengjia Wang is a master student of Nanjing University. Her research focuses on the design and synthesis of fluorescent probes.

Lin Qiu is an associate professor of Changzhou University. Her research interests are fluorescent sensing and nano-systems for theranostic application.

Shuangying Hao is a PhD student of Nanjing University. Her research interest is pathology of Friedreich's ataxia.

Kuanyu Li is a professor of Nanjing University. Her research interests are the pathology of Friedreich's ataxia, and intracellular iron metabolism.

ZijianGuo is a professor of Nanjing University. His research interests include metal-based drugs and the related delivery systems, chemical biology of transition metals, and photoluminescence imaging.

Weijiang He is a professor of Nanjing University. His research interests are photoluminescence imaging, and photo-activated materials and drugs.